Sub-optical-cycle light-matter energy transfer in molecular vibrational spectroscopy

Martin Peschel
Ludwig-Maximilians-Universität
Maximilian Högner
Max-Planck-Institut für Quantenoptik
Theresa Buberl
Max-Planck-Institut für Quantenoptik
Daniel Keefer
University of California, Irvine https://orcid.org/0000-0001-5941-5567
Regina de Vivie-Riedle
Ludwig-Maximilians-Universität München https://orcid.org/0000-0002-7877-5979
Ioachim Pupeza (✉ ioachim.pupeza@mpq.mpg.de)
Max-Planck-Institut für Quantenoptik https://orcid.org/0000-0001-8422-667X

Article

Keywords:

Posted Date: June 14th, 2022

DOI: https://doi.org/10.21203/rs.3.rs-1691869/v1

Sub-optical-cycle light-matter energy transfer in molecular vibrational spectroscopy

Martin T. Peschel[1,*], Maximilian Högner[2,*], Theresa Buberl[2,*], Daniel Keefer[1,4],

Regina de Vivie-Riedle[1✉], Ioachim Pupeza[2,3✉]

1. Ludwig-Maximilians-Universität München, Butenandtstraße 5-13, 81377 Munich, Germany

2. Max-Planck-Institut für Quantenoptik, Hans-Kopfermann-Straße 1,85748 Garching, Germany

3. Ludwig-Maximilians-Universität München, Am Coulombwall 1, 85748 Garching, Germany

4. Department of Chemistry, University of California, Irvine, CA *92697, USA*

** these authors contributed equally*

✉ *corresponding authors*

The evolution of ultrafast-laser technology has steadily advanced the level of detail in studies of light-matter interactions. Here, we employ electric-field-resolved spectroscopy and quantum-chemical modelling to precisely measure and describe the complete coherent energy transfer between octave-spanning mid-infrared waveforms and vibrating molecules in aqueous solution. The sub-optical-cycle temporal resolution of our technique reveals alternating absorption and (stimulated) emission on a few-femtosecond time scale. This behaviour can only be captured when effects beyond the rotating wave approximation (RWA) are included in simulations using first-order time-dependent perturbation theory. At a timescale of femtoseconds to picoseconds, other energy transfer processes are observed, namely optical-phase-dependent coherent transients and the dephasing of the vibrations of resonantly excited methylsulfonylmethane ($DMSO_2$) molecules due to their motion through varying environments in the solvent. *Ab-initio* modelling using density functional theory traces these dynamic processes back to molecular-scale sample properties. The absorbed and coherently re-emitted fractions of the optical energy impinging on the sample can be used as performance metrics for spectroscopic techniques that allow for the separation of absorption and re-emission in time and/or in space. The extension of our study to nonlinear interrogation of higher-order susceptibilities is fathomable with state-of-the-art lasers in the near future.

Static or vibrationally-induced asymmetric charges in molecules cause electric dipole moments, responsible for efficient coupling to infrared (IR) radiation[1]. Optical energy transferred from an excitation IR field to vibrating molecules can either dissipate incoherently in the form of heat, or can be re-emitted with a fixed phase relation to the excitation field, i.e., coherently. Traditional frequency-domain vibrational spectroscopy methods such as direct-absorption spectroscopy or Fourier-transform spectroscopy provide wavelength-resolved absorbance (and phase) information, obtained via temporal integration over the duration of the interaction[2–4]. Fig. 1a illustrates the result of such a measurement for a Lorentzian-shaped absorption line which is typical for linearly-interrogated, homogeneously-broadened resonances of molecules embedded in a solvent[5].

IR molecular absorption spectra contain rich information about molecular composition, abundance and conformation, making vibrational spectroscopy a widely-applied tool in fields including fundamental science[1,6], analytical chemistry[7] and the life sciences[2,8]. However, in traditional frequency-domain spectroscopy, temporal integration hides the transient energy transfer between the light field and the material sample, obscuring deeper insight into the underlying dynamic light-matter interaction.

In this Letter, we report the first quantitative study of the complete energy transfer dynamics between broadband mid-IR optical waveforms and vibrating molecules in aqueous solution, with sub-optical-cycle temporal resolution. Field-resolved IR spectroscopy[9] permits the differentiation between the qualitatively different transient energy transfer for few-cycle excitation (FCE) and chirped-pulse excitation (CPE). FCE allows for temporal separation between absorption and emission, two processes that are qualitatively different in that only coherent re-emission is affected by solvation dynamics. For CPE, additional coherent transients emerge.[10–12] These are caused by the interference between the resonant system response and the non-resonant part of the chirped light wave, which causes additional series of absorption and emission. The discussed effects are quantitatively described by the macroscopic sample susceptibility, which is determined by the microscopic vibrational transition dipole moments, eigenfrequencies and dephasing times of the vibrational modes.[13–16]

Here, we define *absorption* and *coherent emission* as events of energy transfer from the impinging coherent light beam to the molecules and vice versa. For FCE (Fig. 1b), the events of absorption and coherent emission (in analogy to the nuclear magnetic resonance phenomenon of *free induction decay*[10]) are separated in time to a large extent (Fig. 1c-d). While the absorption event is governed by an interference between the excitation waveform and the molecular response, the coherent emission consists only of the latter (after the decay of the excitation). The brevity of the absorption event implies little spectral specificity. In fact, for a Dirac-like excitation, the absorption information reduces to a frequency-independent scalar equal to the total oscillator strength of the sample in the spectral region covered by the excitation. In contrast, the emitted field after FCE contains the frequency-dependent sample-specific spectroscopic information. The ratio of its integrated energy to the excitation energy (Fig. 1e, yellow) is indicative of the "efficiency" with which spectroscopic information can be extracted from the sample. It depends on the environment-dependent transition dipole moments and dephasing times of the molecular sample. The ratios of the maximum absorbed as well as coherently re-emitted energy to the excitation energy are plotted in Fig. 1e as functions of the duration of a Gaussian FCE, showing that FCEs can be regarded as Dirac-like for pulse durations below one tenth of the typical Lorentzian decay time (in our experiment, hundreds of femtoseconds).

In our experiment, the 1-µm pulses of an Yb:YAG thin-disk oscillator were compressed to 15 fs, subsequently driving intrapulse difference-frequency generation in a nonlinear crystal. This resulted in

waveform-stable IR pulses covering the 850-to-1670-cm^{-1} spectral range, which were transmitted through a 30-µm liquid cuvette containing either pure water (reference measurement) or a 10-mg/ml solution of methylsulfonylmethane ($DMSO_2$) in water (sample measurement).

After transmission through the liquid cuvette, the waveforms were recorded via electro-optic sampling[9] (see also Supplementary Information). In a first experiment, the reference waveform was compressed to a duration of 62.5 fs (Fig. 2a). Fig. 2b shows the corresponding sample absorbance, dominated by the resonances of the asymmetric and symmetric stretching vibrations of the SO_2 group.

Temporal integration of the instantaneous intensity difference between reference and sample signals from a time instant t_0 well before the pulse until the (variable) instant t yields the coherent energy transfer between sample and light field, $\mathrm{CET}(t)$ (Fig. 2c):

$$\mathrm{CET}(t) = \int_{t_0}^{t} \left(I_{\mathrm{ref}}^{\mathrm{inst}}(t') - I_{\mathrm{sam}}^{\mathrm{inst}}(t') \right) \mathrm{d}t', \qquad (1)$$

where $I_{\mathrm{ref,sam}}^{\mathrm{inst}}(t) = c\varepsilon_0 \left| \mathcal{E}_{\mathrm{ref,sam}}(t) \right|^2$ is the instantaneous intensity, defined as the magnitude of the Poynting vector, with the real electric field $\mathcal{E}_{\mathrm{ref,sam}}(t)$. This macroscopic quantity is identical to the microscopic coherent energy transfer between the light field and individual molecules, if the pure-water reference measurement is taken as the excitation waveform instead of the actual, propagation-dependent electric field (see Supplementary Information). The level asymptotically approached by $\mathrm{CET}(t)$ for $t \to \infty$ corresponds to the integrated difference of the energy spectral density (ESD) measured in frequency-domain spectroscopy (cf. purple shaded area in Fig. 2b). In our measurement, around 12 % of the absorbed energy (0.6 % of the impinging energy) is coherently re-emitted (Fig. 2c). For a laser pulse described by a Dirac delta function, we obtained a value of 9 % using the ab-initio numerical model (see Supplementary Information), confirming that our experimental conditions are close to a Dirac-like excitation regime.

In a second experiment, we used a 5-mm-thick CaF substrate in the IR beam path to chirp the excitation pulse (Fig. 3a). This leads to a longer pulse duration, such that in contrast to the FCE, a significant portion of the coherent emission now overlaps temporally with the excitation pulse. While the time-integrated ESD (Fig. 3b) yields absorbance information equivalent to that obtained in the FCE case, evaluating the coherent energy transfer with Eq. 1 reveals oscillations in $\mathrm{CET}(t)$ which are not observed in the case of the FCE (Fig. 3c). The maxima of these oscillations around 500 fs and 800 fs can be attributed to the symmetric stretching vibration and the one around -100 fs to the asymmetric stretching vibration. The first oscillation maxima are clearly visible, the later maxima of the asymmetric stretch overlap with the signal due to the symmetric stretch. The oscillations are damped by dephasing and by the pulse intensity decreasing over time.

The emerging alternating sequence of absorption and coherent emission, also known as coherent transients[17] was previously observed for atomic transitions in the visible spectral range[11,12,18,19]. It is caused by the fact that after the resonant transition, the phase of the chirped pulse shifts with respect to the phase of the oscillating system. Whether emission or absorption occurs, depends on the current phase relationship. A more detailed look at $\mathrm{CET}(t)$ (Fig. 3d) reveals an underlying sub-optical-cycle nature of these dynamics: energy is absorbed or emitted in a stepwise fashion with each half-cycle of the electric field.

To quantitatively explain the energy transfer dynamics observed in the experiment, we built a model based on time-dependent first-order perturbation theory. Under the assumption of a linear sample response (which is experimentally confirmed within the precision of our measurement), according to the optical Bloch equations the susceptibility $\chi^{(1)}(\omega)$ of a molecular solution of concentration β of a molecule of mass *m* is given by[6,20]:

$$\chi^{(1)}(\omega) = \sum_k \frac{2}{3}\frac{\beta}{m\hbar\varepsilon_0}\frac{{\mu_{0k}}^2\omega_k}{\omega_k^2-(\omega-i\Gamma_k)^2} \ . \qquad (2)$$

Thus, in the spectral range covered by our laser field $\mathcal{E}(\mathrm{t})$, each vibrational mode k forms a Lorentz oscillator, parametrized by three parameters: the central frequency ω_i, the transition dipole moment μ_{0k} and the homogeneous dephasing rate Γ_k. We consider all 27 vibrational modes of $DMSO_2$. The parameters ω_k, μ_{0k} and Γ_k can either be fitted to the experimental data, or they can be determined by *ab-initio* quantum-chemical calculations. The simulation curves shown in Fig. 2b,c and Fig. 3c,d were obtained from the total susceptibility as described in the Supplementary Information.

In a time-domain description, the interaction of the laser field $\mathcal{E}(\mathrm{t})$ with each vibrational mode leads to a coherence[6]

$$\rho_{0\mathrm{k}}^{(1)}(\mathrm{t}) = \frac{i}{\hbar}\mu_{0k}\int_0^\infty \mathcal{E}(\mathrm{t}-\mathrm{t}_1)\mathrm{e}^{\mathrm{i}\omega_\mathrm{k}\mathrm{t}_1}\mathrm{e}^{-\Gamma_\mathrm{k}\mathrm{t}_1}\mathrm{d}\mathrm{t}_1, \qquad (3)$$

which causes a polarization

$$\mathrm{P}_\mathrm{k}^{(1)}(\mathrm{t}) = F^{-1}\{\varepsilon_0\cdot{\chi_k}^{(1)}(\omega)\cdot\mathcal{E}(\omega)\}(t) = \frac{2}{3}\frac{\beta N_A}{M}\mu_{0k}\,Re(\rho_{0\mathrm{k}}^{(1)}). \qquad (4)$$

The fields thus created from each infinitesimal sample ($DMSO_2$ molecules and their immediate solvent environment), interfere with each other and with the incident field to create the observed response in the transverse mode of the laser.

The curves in Fig. 4a-c show the evolution of the coherence of one exemplary vibrational mode, the symmetric stretching vibration, in the complex plane, calculated using Eq. 3. One may invoke the RWA[21], which neglects terms oscillating with the sum of the vibrational and field frequencies to obtain the curves in Fig. 4a,c. However, field-resolved spectroscopy resolves sub-optical-cycle dynamics, directly revealing the influence of these terms. It is evident comparing Fig. 4a to Fig. 4b and Fig. 4c to

Fig. 4d that the sub-cycle dynamics vanish under the RWA. The term neglected in the RWA imprints a cycloid structure onto the polarization, which corresponds to the step-like patterns and sub-cycle oscillations in Fig. 3c.

The coherent transients observed with CPE are illustrated by the spiral shapes in Fig. 4c,d, when considering that $\mathrm{CET}(t)$ in Fig. 3 is proportional to the squared absolute value of the coherence (see Supplementary Information). The system starts at $t = t_0$ in equilibrium at the origin. Then, the chirped pulse interacts with the system. At first, this interaction is off-resonant, which leads to a spiraling around the origin with increasing amplitude and decreasing frequency, as resonance is approached. This spiral corresponds to a slow increase of $\mathrm{CET}(t)$ in Fig. 3 at early times. At resonance, a large increase in the magnitude of the coherence is observed. Finally, the off-resonant interaction once more leads to a spiral pattern, which manifests as the damped oscillation in Fig. 3 at later times, as the magnitude of the polarization increases and decreases with each loop. Thus, the contributions of the non-resonant excitation to the complex amplitude cause the sequence of absorption and stimulated emission.

The *ab-initio* model permits an in-depth study of the influence of the surrounding solvent on the vibrating molecules. Specifically, we used the M06-2X density functional[13] to calculate transition frequencies and transition dipole moments of a single molecule without an environment, a single molecule embedded in a polarizable continuum model (PCM) or in different $DMSO_2$-water clusters embedded in a PCM. We focused on the symmetric and asymmetric stretching vibration of the SO_2 moiety, which are the main modes contributing in the observed spectral range (Fig. 2b). The transition frequency distribution of the $DMSO_2$-water clusters demonstrates that the observed dephasing is mainly due to the dynamics of the molecule in the solvent (homogeneous broadening) and not due to their static structure (inhomogeneous broadening). This agrees with the experimentally observed Lorentzian line shapes, which can also be observed in *ab-initio* molecular dynamics simulations (see Supplementary Information).

For the symmetric stretching vibration without environment, an absorption frequency of 1192 cm^{-1} is predicted, which is higher than the experimentally measured value in solution of 1135 cm^{-1}. The inclusion of a PCM shifts the absorption maximum to 1142 cm^{-1}, the inclusion of explicit water molecules to 1148 cm^{-1}. For the transition dipole moments, the environment-free calculation predicts a value of 0.24 D which is considerably lower than the measured value of 0.30 D. The inclusion of a PCM changes the predicted value to 0.32 D, that of explicit water to 0.33 D. The frequencies for the asymmetric stretching vibration behave similarly to the symmetric stretching vibration: the predicted environment-free value (1311 cm^{-1}) is considerably higher than the experimental value (1280 cm^{-1}). The inclusion of a PCM reduces the transition frequencies to 1288 cm^{-1}, including explicit water

molecules to 1301 cm^{-1}. In summary, due to solvation, absorption maxima are red-shifted, and transition dipole moments increase significantly.

Examining partial charges of the oxygen atoms in the density-functional-theory simulations shows that the environment reduces the electrostatic interaction between different parts of the molecule, leading to a more asymmetric charge distribution. This causes higher dipole moments and less rigid bonds. The static polarizability of the solvent environment thus enhances the molecule-field interaction. This effect is equally well described by both the explicit solvent model and the PCM. However, with the explicit solvent model the molecular dynamics of the entire system can be simulated, which provides qualitative estimates of the dephasing rate Γ (see Eq. 2 and Supplementary Information).

In conclusion, sub-optical-cycle-temporal-resolution field-resolved spectroscopy together with *ab initio* modelling provides quantitative, molecular-scale insight into the complete coherent energy transfer dynamics between broadband infrared light and vibrating molecules in solution. For an ultra-brief, broadband excitation, time-domain detection allows for the distinction between two qualitatively different light-matter energy transfer regimes: *Absorption* is governed by the strengths of the transition dipole moments for each individual molecule, independently. The generation of vibrational coherence with each half-cycle of the electric field is resolved. *Emission* yields a coherent sample-specific "spectroscopic fingerprint" carrying dephasing information due to molecular motion in varying environments. For spectroscopic techniques that allow for the separation of these two regimes in time[9,22,23] or in space[24,25], the ratio of the coherently transferred optical energy to the excitation energy (Fig. 4e) provides an indicator for the required spectroscopic detection sensitivity. For example, for our test molecule $DMSO_2$ at physiolocically-relevant[26] sub-ng/ml concentrations in water, the energy coherently re-emitted as a spectroscopic fingerprint amounts to $<10^{-16}$ of the excitation energy (and to $<10^{-8}$ of the absorbed energy), providing quantitative guidelines for the design of corresponding spectroscopic experiments. Our experimentally-validated *ab-initio* model directly connects these energy transfer ratios to electrostatic and dynamic solvent interactions, thereby fully tracing them back to molecular-scale properties of the sample.

The peak field strengths of less than 75 kV/cm in our experiment populate the first excited state only on the order of 10^{-3}, rendering nonlinearities in the sample response negligible. With the availability of high-intensity, broadband, waveform-stable mid-IR sources[27–30] the extension of our study to field-resolved nonlinear (multidimensional) coherent spectroscopies[6,31–33] in the molecular fingerprint region becomes promising in the near future. This would enable studies of the coupling between vibrational modes and of the correlation functions describing the fluctuating environments using phase-sensitive direct observation of the electrical field with unprecedented time resolution.

Acknowledgements

We thank Ferenc Krausz and Marinus Huber for useful discussions. This research was undertaken thanks, in part, to funding from the Technology Transfer Program of the Max Planck Society, the Max Planck-UBC-UTokyo Center for Quantum Materials**.** R.d.V.-R. acknowledges funding by the German Research Foundation (DFG) under Germany's excellence strategy EXC 2089/1-39077620.

Author contributions

M.T.P, M.H., T.B., R.d.V.-R. and I.P. designed the experiments and the theoretical framework. T.B. performed the experiments. T.B. and M.H. analysed the experimental data. M.T.P. and D.K. performed the density functional theory simulations. M.H. and M.T.P. developed the model and analysed the simulation data. M.T.P, M.H. and I.P. wrote the manuscript with input from all other authors. I.P. and R.d.V.-R. supervised the project.

Data and materials availability

All data in the main text or the supplementary materials is available from the authors upon reasonable request.

Competing interests

The authors declare that they have no competing interests.

References

1. Demtröder, W. *Molecular Physics*. (Wiley-VCH Verlag GmbH, 2005).
2. Griffiths, P. R. & De Haseth, J. A. *Fourier transform infrared spectrometry*. (Wiley-Interscience, 2007).
3. Hayden, J., Hugger, S., Fuchs, F. & Lendl, B. A quantum cascade laser-based Mach–Zehnder interferometer for chemical sensing employing molecular absorption and dispersion. *Applied Physics B* **124**, (2018).
4. Picqué, N. & Hänsch, T. W. Frequency comb spectroscopy. *Nature Photon* **13**, 146–157 (2019).
5. Laubereau, A. & Kaiser, W. Vibrational dynamics of liquids and solids investigated by picosecond light pulses. *Reviews of Modern Physics* **50**, 607–665 (1978).
6. Mukamel, S. *Principles of Nonlinear Optical Spectroscopy*. (Oxford University Press, Inc., 1995).
7. Haas, J. & Mizaikoff, B. Advances in Mid-Infrared Spectroscopy for Chemical Analysis. *Annual Review of Analytical Chemistry* **9**, 45–68 (2016).
8. Baker, M. J. *et al.* Using Fourier transform IR spectroscopy to analyze biological materials. *Nature Protocols* **9**, 1771–1791 (2014).
9. Pupeza, I. *et al.* Field-resolved infrared spectroscopy of biological systems. *Nature* **577**, 52–59 (2020).
10. Jacobsohn, B. A. & Wangsness, R. K. Shapes of Nuclear Induction Signals. *Phys. Rev.* **73**, 942–946 (1948).
11. Rothenberg, J. E. & Grischkowsky, D. Measurement of the phase of a frequency-swept ultrashort optical pulse. *Journal of the Optical Society of America B* **2**, 626 (1985).
12. Zamith, S. *et al.* Observation of Coherent Transients in Ultrashort Chirped Excitation of an Undamped Two-Level System. *Physical Review Letters* **87**, 033001 (2001).
13. Zhao, Y. & Truhlar, D. G. The M06 suite of density functionals for main group thermochemistry, thermochemical kinetics, noncovalent interactions, excited states, and transition elements: two new functionals and systematic testing of four M06-class functionals and 12 other functionals. *Theor Chem Account* **120**, 215–241 (2008).

14. Li, S., Schmidt, J. R., Corcelli, S. A., Lawrence, C. P. & Skinner, J. L. Approaches for the calculation of vibrational frequencies in liquids: Comparison to benchmarks for azide/water clusters. *The Journal of Chemical Physics* **124**, 204110 (2006).
15. Thomas, M., Brehm, M., Fligg, R., Vöhringer, P. & Kirchner, B. Computing vibrational spectra from ab initio molecular dynamics. *Phys. Chem. Chem. Phys.* **15**, 6608 (2013).
16. Thomas, M., Brehm, M. & Kirchner, B. Voronoi dipole moments for the simulation of bulk phase vibrational spectra. *Phys. Chem. Chem. Phys.* **17**, 3207–3213 (2015).
17. del Campo, A., García-Calderón, G. & Muga, J. G. Quantum transients. *Physics Reports* **476**, 1–50 (2009).
18. Rothenberg, J. E. & Grischkowsky, D. Subpicosecond transient excitation of atomic vapor and the measurement of optical phase. *Journal of the Optical Society of America B* **3**, 1235 (1986).
19. Monmayrant, A., Chatel, B. & Girard, B. Quantum state measurement using coherent transients. *Physical Review Letters* **96**, 2–5 (2006).
20. Andreev, S. N., Mikhailov, A. V, Ochkin, V. N., Pestovskiy, N. V & Savinov, S. Y. Self-radiation of an absorbing medium induced by a fast frequency-tuning laser. *Laser Physics* **25**, 025701 (2015).
21. Agarwal, G. S. Rotating-Wave Approximation and Spontaneous Emission. *Physical Review A* **4**, 1778–1781 (1971).
22. Kowligy, A. S. *et al.* Infrared electric field sampled frequency comb spectroscopy. *Sci. Adv.* **5**, eaaw8794 (2019).
23. Lanin, A. A., Voronin, A. A., Fedotov, A. B. & Zheltikov, A. M. Time-domain spectroscopy in the mid-infrared. *Scientific Reports* **4**, (2015).
24. Buberl, T., Sulzer, P., Leitenstorfer, A., Krausz, F. & Pupeza, I. Broadband interferometric subtraction of optical fields. *Opt. Express* **27**, 2432 (2019).
25. Tomberg, T., Muraviev, A., Ru, Q. & Vodopyanov, K. L. Background-free broadband absorption spectroscopy based on interferometric suppression with a sign-inverted waveform. *Optica* **6**, 147 (2019).

26. Geyer, P. E., Holdt, L. M., Teupser, D. & Mann, M. Revisiting biomarker discovery by plasma proteomics. *Molecular Systems Biology* **13**, 942, 1–15 (2017).
27. Junginger, F. *et al.* Single-cycle multiterahertz transients with peak fields above 10 MV/cm. *Optics Letters* **35**, 2645 (2010).
28. Schubert, O. *et al.* Sub-cycle control of terahertz high-harmonic generation by dynamical Bloch oscillations. *Nature Photonics* **8**, 119–123 (2014).
29. Gaida, C. *et al.* Watt-scale super-octave mid-infrared intrapulse difference frequency generation. *Light: Science & Applications* **7**, (2018).
30. Elu, U. *et al.* Seven-octave high-brightness and carrier-envelope-phase-stable light source. *Nat. Photonics* **15**, 277–280 (2021).
31. Hamm, P. & Zanni, M. *Concepts and Methods of 2D Infrared Spectroscopy*. (Cambridge University Press, 2011). doi:10.1017/CBO9780511675935.
32. Hamm, P. & Shalit, A. Perspective: Echoes in 2D-Raman-THz spectroscopy. *The Journal of Chemical Physics* **146**, 130901 (2017).
33. Baiz, C. R. *et al.* Vibrational Spectroscopic Map, Vibrational Spectroscopy, and Intermolecular Interaction. *Chem. Rev.* **120**, 7152–7218 (2020).

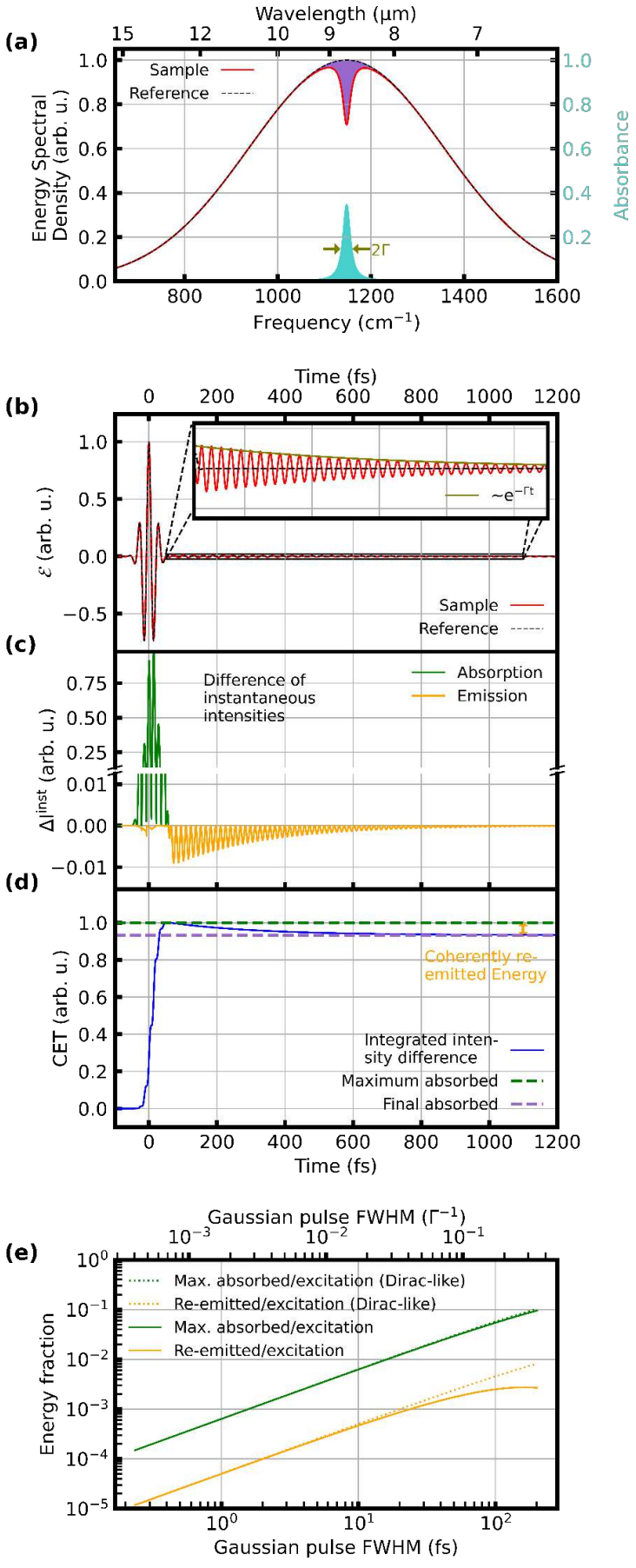

Figure 1. Time-integrated and time-resolved broadband vibrational spectroscopy. a, Model spectrum before (black, dashed) and after (red) transmission through a Lorentzian absorber centred at 1147 cm-

[1] with a full-width-at-half-maximum (FWHM) of 115 cm^{-1}, shown for conventional (time-integrating) absorption spectroscopy. Purple shaded area: difference between the two spectra, amounting to the energy incoherently dissipated in the molecular sample. Turquoise shaded area: normalized absorbance, defined as the difference between the logarithms of the two spectra per unit sample length *z*; *(log(|Reference|)-log(|Sample|))/z*. **b,** Electric field $\boldsymbol{\mathcal{E}(t)}$ of the 30-fs-full-width-half-maximum Gaussian excitation pulse (black, dashed) with the spectrum shown in black in (a). Red: coherent response of the Lorentzian absorber shown in (a) to this few-cycle excitation (FCE). **c,** Time-resolved difference $\boldsymbol{\Delta I^{inst}(t)}$ of the instantaneous intensities of the electric fields in (b). The positive values (green) correspond to absorption, the negative values (yellow) to coherent emission. For FCE, the coherent emission event has no contribution from the excitation. **d,** Integration of $\boldsymbol{\Delta I^{inst}(t)}$ shown in (c) yields the coherent energy transfer $\boldsymbol{CET(t)}$. Green dashed line: maximum of $\boldsymbol{CET(t)}$, i.e., the maximum transiently absorbed energy. Purple dashed line: end value of $\boldsymbol{CET(t)}$, equal to the purple shaded area in (a). Orange double arrow: difference between maximum and end value, corresponding to the energy which is coherently re-emitted by the Lorentzian absorber. **e,** Ratio of the maximum transiently absorbed energy (green) and the coherently-re-emitted energy (yellow) to the excitation pulse energy, as a function of the FCE-pulse duration. These ratios deviate by less than 20% from a Dirac-like excitation (dotted lines, see also Supplementary Information) for pulse durations below one tenth of the typical Lorentzian decay time $\boldsymbol{\Gamma^{-1}}$ (here, 580 fs).

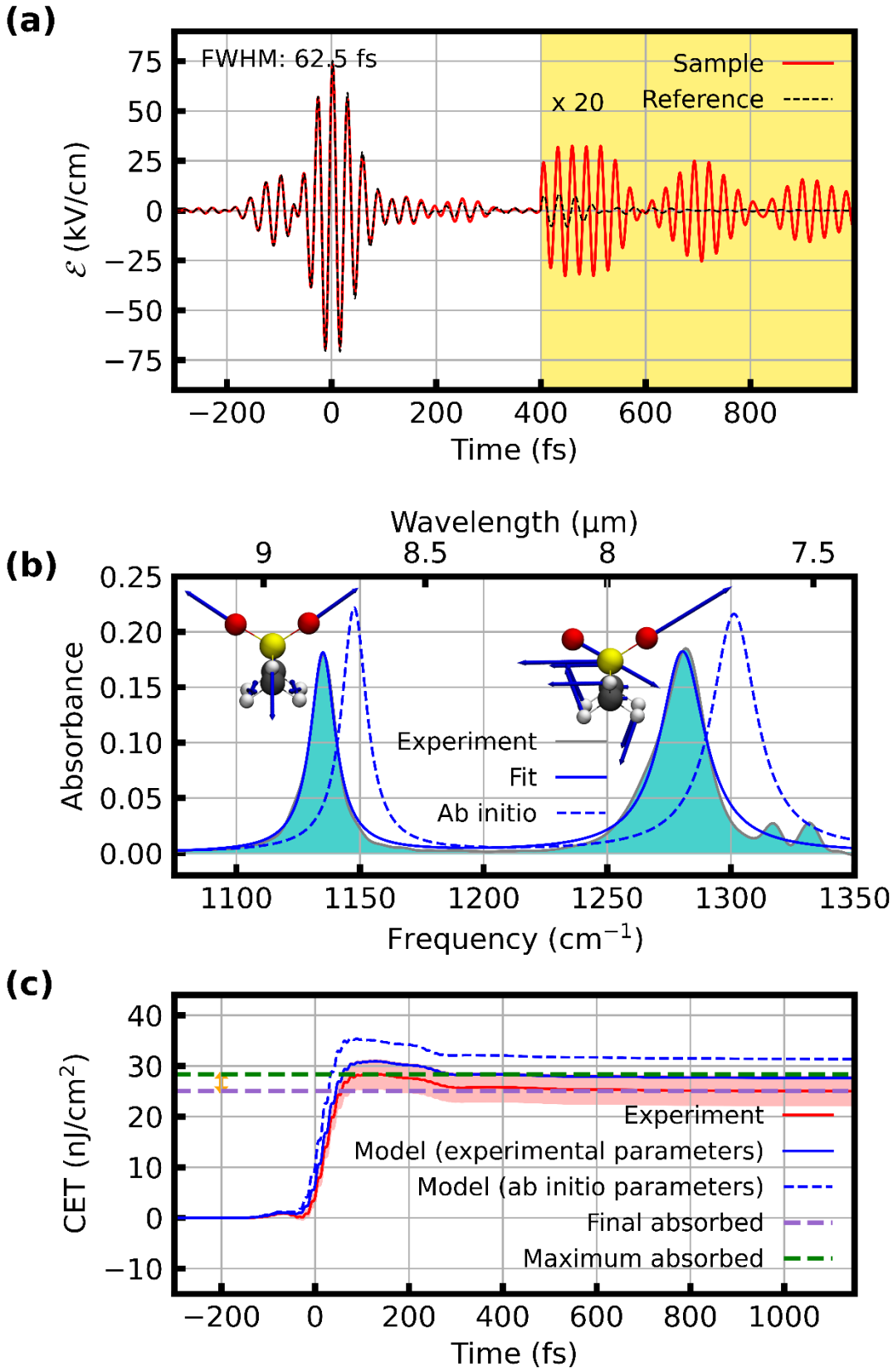

Figure 2. Few-cycle excitation (FCE). a, Electric field of the compressed excitation pulse after transmission through a 30-μm thick layer of water (black, dashed) and a solution of 10 mg/ml $DMSO_2$ in water (red). **b,** Absorbance derived from the measurements in (a). The insets illustrate the corresponding displacement vectors of the vibrational modes responsible for the two main absorption

bands, the symmetric (left) and asymmetric (right) SO_2 stretching vibrations. Solid blue: Lorentzian fits, dashed blue: ab-initio calculations (see text). **c,** Coherent energy transfer $\mathrm{CET}(t)$ between the excitation field and the $DMSO_2$ sample, extracted from the experimental data (solid red line: mean value of five consecutive measurements comprising 10 scans each, shaded red area: standard deviation of five consecutive measurements), from modelling with the fitted Lorentzian parameters (solid blue line), and with Lorentzian parameters obtained *ab initio* (dashed blue line). The dashed green and purple lines show the maximum and end level of the CET, respectively. Their difference is the coherently emitted energy, which is 12% of the maximum absorbed energy (orange double arrow).

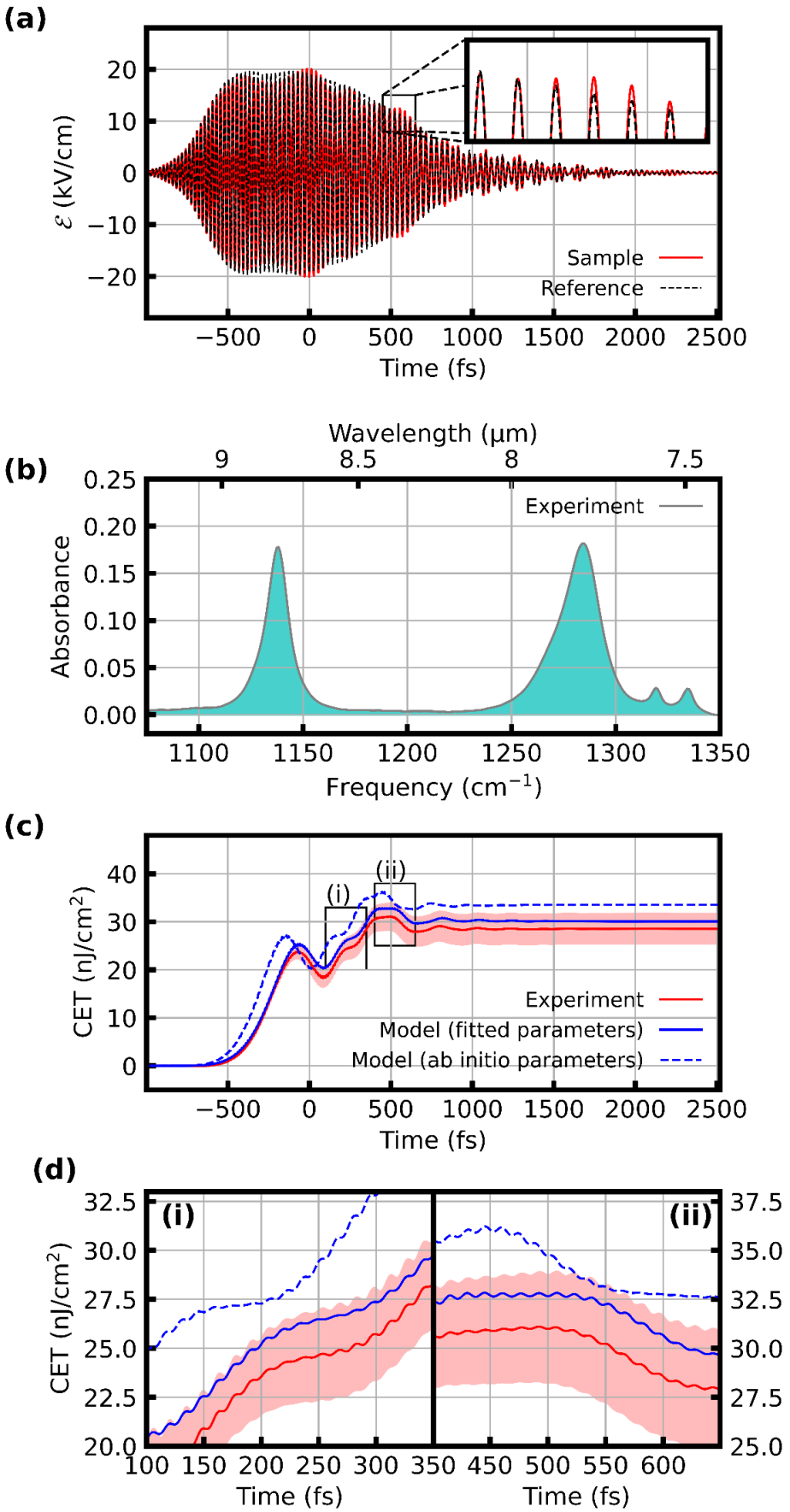

Figure 3. Chirped-pulse excitation (CPE). a, Electric field of the chirped excitation pulse after transmission through a 30-μm thick layer of water (black, dashed) and 10-mg/ml solution of $DMSO_2$ in

water (red). **b,** Absorbance, calculated from the measurements in (a). **c,** Coherent energy transfer $\mathrm{CET}(t)$ between the excitation field and the $DMSO_2$ solution, extracted from the experimental data (solid red line: mean value of five consecutive measurements, shaded red area: standard deviation of five consecutive measurements comprising 10 scans each), from modelling with the fitted Lorentzian parameters (solid blue line, see Fig. 2), and with Lorentzian parameters obtained *ab initio* (dashed blue line). **d,** Magnified displays of the sections encased by the dashed black rectangles (i) and (ii) in (c), revealing the sub-optical-cycle structure of absorption and stimulated emission.

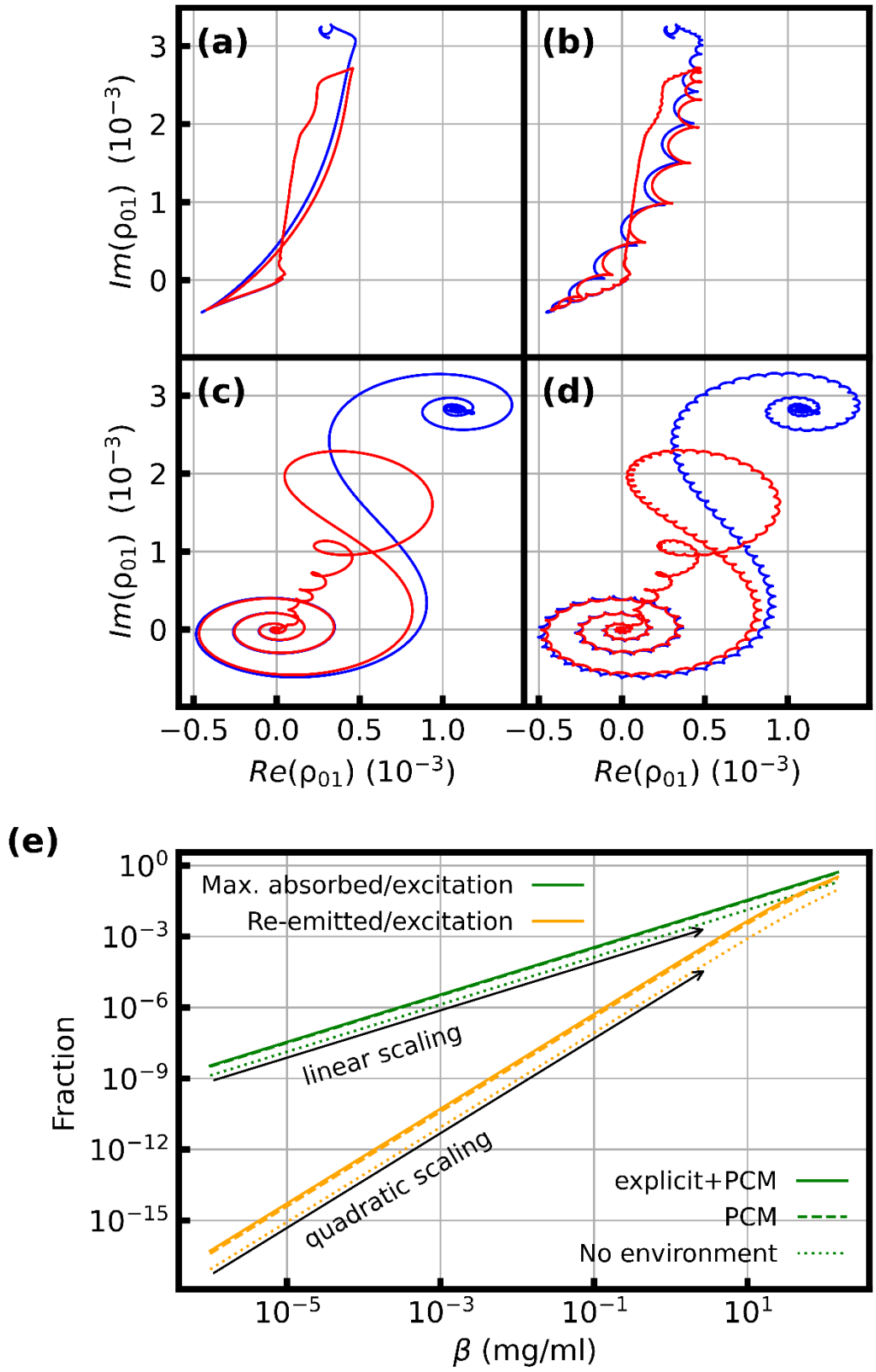

Figure 4. Calculated coherence and energy transfer ratios. a-d, Calculated vibrational molecular coherence in the asymmetric stretching vibrational mode of the $DMSO_2$ molecule in solution displayed in a frame rotating with the vibrational eigenfrequency. The calculations are done with (a) the compressed pulse using the RWA, (b) the compressed pulse without the RWA, (c) the chirped pulse using the RWA, and (d) the chirped pulse without the RWA. The red curves include relaxation; the blue

curves do not include relaxation. Each “bump” of the cycloid in (b) corresponds to one half-cycle of the electric field, showing that energy transfer from the excitation field to the molecular system is completed after 3 to 4 field cycles (Fig. 2b) in the case of the FCE. **e,** re-emitted (orange) and maximum absorbed (green) fraction of the impinging pulse energy versus concentration. The results were obtained from the delta-pulse model (see Supplementary Information) with the FCE and ab-initio Lorentz parameters. The solid lines include direct interactions with the surrounding water and the screening effect of the polarizable continuum, the dashed lines only the latter, and the dotted lines neither. For small concentrations, the maximum absorbed energy scales linearly with the concentration, and the coherent re-emission, containing the spectroscopic information, scales quadratically with the concentration, due to the absence of homodyning with the excitation field (see Supplementary Information). This scaling behaviour is in line with the Beer-Lambert law and derives from the linear relationship between the concentration and the amplitude difference caused by the sample. The fraction of re-emitted energy also depends on the line strengths, which are affected by interactions with the solvent.

Supplementary Files

This is a list of supplementary files associated with this preprint. Click to download.

- 20220602EnergytransferSI.docx